Secondary Envelopment of Human Cytomegalovirus Is a Fast Process Utilizing the Endocytic Compartment as a Major Membrane Source

Tim Bergner , Laura Cortez Rayas , Gesa Freimann , Clarissa Read , Jens von Einem *

Posted Date: 23 August 2024

doi: 10.20944/preprints202408.1752.v1

Keywords: herpesvirus morphogenesis; plasma membrane labelling; HCMV; TEM; STEM

Article

Secondary Envelopment of Human Cytomegalovirus is a Fast Process Utilizing the Endocytic Compartment as a Major Membrane Source

Tim Bergner [1], Laura Cortez Rayas [2], Gesa Freimann [1], Clarissa Read [1,*] and Jens von Einem [2,*]

[1] Central Facility for Electron Microscopy, Ulm University, Ulm, Germany; tim.bergner@uni-ulm.de; gesa.freimann@web.de

[2] Institute of Virology, Ulm University Medical Center, Ulm, Germany; laura.cortez-rayas@uni-ulm.de

* Correspondence: clarissa.read@uni-ulm.de; jens.von-einem@uni-ulm.de

Abstract: Secondary envelopment of the human cytomegalovirus (HCMV) is a critical but not well-understood process that takes place at the cytoplasmic viral assembly complex (cVAC) where nucleocapsids acquire their envelope by budding into cellular membranes containing viral glycoproteins. Previous studies presented controversial results regarding the composition of the viral envelope, suggesting trans-Golgi and endosomal origins, as well as intersections with the exosomal and endocytic pathways. Here, we investigated the role of endocytic membranes for the secondary envelopment of HCMV by using wheat germ agglutinin (WGA) pulse labelling to label glycoproteins at the plasma membrane and to follow their trafficking during HCMV infection by light microscopy and transmission electron microscopy (TEM). WGA labelled different membrane compartments within the cVAC, including early endosomes, multivesicular bodies, *trans*-Golgi, and recycling endosomes. Furthermore, TEM analysis showed that almost 90% of capsids undergoing secondary envelopment and 50% of enveloped capsids were WGA-positive within 90 minutes. Our data reveal extensive remodeling of the endocytic compartment in the late stage of HCMV infection, where the endocytic compartment provides an optimized environment for virion morphogenesis and serves as the primary membrane source for secondary envelopment. Furthermore, we show that secondary envelopment is a rapid process in which endocytosed membranes are transported from the plasma membrane to the cVAC within minutes to be utilized by capsids for envelopment.

Keywords: herpesvirus; morphogenesis; plasma membrane labelling; HCMV; TEM; STEM

1. Introduction

The formation of infectious herpesvirus particles is completed by a cytoplasmic envelopment process in which the capsids acquire a lipid bilayer envelope. This process is referred to as secondary envelopment and is conserved among herpesviruses. Secondary envelopment involves the budding of partially tegumented capsids at intracellular membranes of vesicles and tubules that contain viral glycoproteins, which drives the engulfment of these capsids by membranes. The envelopment process is completed by membrane scission, resulting in virions enclosed by a vesicle membrane. Betaherpesviruses, and in particular human cytomegalovirus (HCMV), also known as human herpesvirus 5 (HHV-5), have been shown to induce reorganization of cellular membrane systems, including Golgi, ER, endosomal, and exosomal membranes, to form a cytoplasmic compartment known as the cytoplasmic viral assembly compartment (cVAC), viral assembly compartment (vAC), or assembly compartment (AC) [1–3]. The cVAC has a unique structure characterized by a specific arrangement of different membrane compartments. These compartments include Golgi stacks that are reorganized to form an outer ring of membranes defining the region of the cVAC and membranes from the secretory and endosomal compartment that are localized towards the center of the cVAC [1,4–8]. The cVAC forms around the centrosomal microtubule organizing center (MTOC), but also functions as an MTOC for non-centrosomal microtubules [9]. One advantage of forming a

 doi:10.20944/preprints202408.1752.v1

compartment such as the cVAC is the concentration of components and parts necessary for the assembly of infectious virions, including capsids, viral proteins, and membranes (reviewed in [10]). The importance of the cVAC for virion assembly is further underscored by the fact that secondary envelopment has only been detected in this region [3] and that defects in cVAC formation result in impaired viral growth [11]. HCMV virions have a complex structure consisting of the DNA genome, an icosahedral capsid, a tegument layer of proteins of viral and cellular origin, and various glycoproteins and glycoprotein complexes embedded in the host cell-derived lipid bilayer envelope [12–14]. While the role of tegument proteins and glycoproteins in secondary envelopment is becoming better understood and the underlying molecular mechanisms are gradually being uncovered, it is still a matter of debate from which compartment of the host cell the HCMV envelope originates. Data from fluid phase endocytic tracer horseradish peroxidase (HRP) experiments in combination with electron microscopy indicated budding of HCMV at membranes of tubular early endosomes [15]. In contrast, immunogold labelling of subcellular markers in HCMV-infected cells suggested that secondary envelopment of HCMV particles takes place mainly at Golgi-derived secretory vacuoles [16]. Subsequent work using immunogold labelling on isolated virus particles demonstrated the incorporation of various subcellular markers, such as the trans-Golgi network (TGN) protein TGN46, the endosomal markers early endosomal antigen 1 (EEA1) and annexin I, the recycling endosome marker transferrin receptor (TfR), the multivesicular body (MVB) marker CD63, and the cation-independent mannose 6-phosphate receptor, into the viral envelope, suggesting generation of a mixed membrane compartment containing TGN, endosomal and exosomal markers [17]. Other herpesviruses have also been shown to utilize Golgi membranes for their secondary envelopment [18–22]. Additionally, it has been demonstrated that endocytic tubules serve as the primary membrane source in herpes simplex virus 1 (HSV-1) infections [23].

Besides relocation and expansion of membrane compartments upon HCMV infection, there is evidence of the formation of mixed membrane compartments during HCMV infection, which complicates an unambiguous identification of the HCMV envelope membrane source [4]. There are several lines of evidence that HCMV utilizes membranes of the endocytic compartment for virion assembly. Several HCMV structural proteins, e.g. glycoproteins B, M (gB, gM), and gpUL132 as well as the tegument protein pUL71, are transported to the plasma membrane of the host cell during infection and then, triggered by endocytic trafficking motifs, transported back to the cVAC via endocytosis [24–27]. For example, the trafficking motifs in the cytoplasmic tail of gM are essential for the formation of infectious virus particles [25]. Similarly, a mutation of the N-terminal YxxΦ trafficking motif of pUL71 leads to an altered intracellular localization of this protein at the plasma membrane and to a defect in virus assembly [26]. Furthermore, it was shown that endocytosis inhibitors significantly reduce HCMV growth rates without affecting early and late viral gene expression [28]. Dynamin, a key component of the endocytic machinery, has an essential role in the early stages of murine cytomegalovirus (MCMV) infection, involving the rearrangement of membranes to form the cVAC, which is critical for virus maturation [29] and late in infection for virus morphogenesis and egress [30].

Together, these data suggest an important role of endocytosed membranes in the secondary envelopment of HCMV and support the hypothesis that the endocytic compartment is the primary source of HCMV envelopment. To better understand the use and extent of viral utilization of the endocytic membrane compartment for the cytoplasmic envelopment of capsids, we characterized the uptake and trafficking of wheat germ agglutinin (WGA) during HCMV infection using fluorescence light microscopy and electron microscopy. WGA is a lectin with a high affinity for N-acetylglucosamine and sialic acid, which is internalized into the cell by endocytosis upon binding to various cellular proteins on the plasma membrane. WGA has been used to label and to study the endocytic compartment in different cell types, including human fibroblasts, and when coupled with horse radish peroxidase (HRP) allows for visualization of the WGA-positive compartment in electron microscopy [31,32]. In this study, we show that HCMV alters the trafficking of endocytosed WGA compared to uninfected cells, resulting in rapid accumulation of WGA-positive membranes at the cVAC region. In contrast to uninfected cells, the WGA-positive compartment at the cVAC was largely

 doi:10.20944/preprints202408.1752.v1

negative for EEA1, indicating viral modulation of endocytic trafficking of cargo beyond early endosomes to provide the membranes for secondary envelopment. WGA-positive membranes at the cVAC, including vesicles and tubules of varying sizes, and trans-most cisternae of Golgi-membrane stacks, were used by nucleocapsid for budding. These findings verified that endocytosed membranes serve as the primary source for the viral envelope. Quantitative analysis of budding capsids at WGA-positive membranes and of enveloped capsids demonstrated that secondary envelopment is a fast and dynamic process. Finally, we found that secondary envelopment of capsids, including endocytosis and transport of membranes, proteins, and capsids to the cVAC, is completed within 30 minutes, demonstrating a first temporal delineation of these processes in HCMV infection. In conclusion, our results imply extensive modulation of the endocytic compartment by HCMV, which serves as the primary source of membranes used by HCMV for secondary envelopment.

2. Materials and Methods

2.1. Cell Culture

Human foreskin fibroblasts were cultivated in fibroblast culture medium consisting of Dulbecco's modified eagle medium (DMEM, Sigma Aldrich) supplemented with 100 units/ml penicillin, 100 µg/ml streptomycin, 10% fetal calf serum (FCS), and 1x non-essential amino acids at 37 °C and 5% CO_2 in a humidified incubator. Fibroblasts were used between passages 20 and 30 for experiments when a confluency of 90-100% was reached.

2.2. Virus

Fibroblasts were infected with HCMV bacterial artificial chromosome (BAC) clone TB40-BAC4 derived from the endotheliotropic HCMV strain TB/40E (accession number EF999921.1; [33]. For all experiments fibroblasts were infected at a multiplicity of infection (MOI) of 1, resulting in an infection rate of around 60%.

2.3. Antibodies

HCMV and cellular proteins were detected in indirect immunofluorescence experiments using mouse monoclonal antibodies directed against *cis*-Golgi protein marker GM130 (clone 35/GM130, BD Transduction Laboratories), early endosome marker EEA1 (clone 14/EEA1, BD Biosciences), multivesicular body (MVB) marker CD63 (clone H5C6, BD Biosciences), TGN markers Golgin97 (clone CDF4, Invitrogen) and ɣ-Adaptin (clone 100/3, Sigma-Aldrich), HCMV pUL99 (clone CH19, Santa Cruz Biotechnology), and HCMV gM (IMP 91-31, kindly provided by Michael Mach, Erlangen-Nürnberg University, Erlangen). TGN marker TGN46 (Novus) and HCMV pUL71 [3] were detected with rabbit polyclonal antibodies. BrdU was then detected using a rat anti-BrdU monoclonal antibody (RF06, Bio-Rad) and an anti-rat secondary antibody coupled to Alexa Fluor 555 (Invitrogen). Goat anti-rabbit and goat anti-mouse antibodies conjugated to either Alexa Fluor 555 or Alexa Fluor 647 (Invitrogen) were used as secondary antibodies.

2.4. Fluorescence Microscopy

To label endocytic membranes and the recycling compartment in HCMV-infected fibroblasts, we used fluorescence-labelled WGA (WGA-FITC) and transferrin (Tf-AF555), respectively. Fibroblasts were seeded in µ-Slide 18-well chamber slides (ibidi GmbH, Germany) and infected the following day. Pulse-chase labelling was performed at 120 hours post-infection (hpi) by incubating the cells with WGA-FITC (10 µg/ml) at 37 °C for 60 minutes or with WGA-FITC (20 µg/ml) at 4 °C (on ice) for 10 minutes (pulse). In experiments in which the endocytic and the recycling compartment were labelled, infected fibroblasts were incubated simultaneously with WGA-FITC (10 µg/ml) and Tf-AF555 (50 µg/ml) for 60 minutes at 37 °C. After that, the labelling solutions were exchanged with fresh fibroblast culture medium. Fibroblasts were then incubated for 30 minutes at 37 °C (chase). For the endocytosis inhibition control both, pulse and chase, were performed at 4 °C (on ice).

Subsequently, the cells were washed with PBS followed by fixation with 4% paraformaldehyde (PFA) in PBS for 10 minutes at 4 °C. Indirect immunofluorescence staining was performed as

 doi:10.20944/preprints202408.1752.v1

previously described [26]. In short, cells were permeabilized with 0.1% Triton X-100 in PBS for 10 minutes at room temperature followed by blocking of unspecific binding sites with a blocking solution containing 1% bovine serum albuminutes and 10% horse serum in PBS for 30 minutes at room temperature. Primary and secondary antibodies were diluted in blocking solution. Cell nuclei were stained with 0.33 µg/ml 4,6-diamidino-2-phenylindole (DAPI, Sigma-Aldrich). Confocal images were acquired with a 63x objective lens of the Axio-Observer.Z1 fluorescence microscope equipped with an ApoTome (Zeiss) and images were processed with ZEN 3.7 pro (Zeiss).

Nucleocapsids were detected via pulse labelling of newly synthesized DNA with thymidine analog 5-bromo-2'-deoxyuridine (BrdU, Thermo Fisher Scientific). To this end, HCMV-infected fibroblasts were incubated with a 10 µM BrdU solution at 37 °C 24 hours before fixation of cells for light microscopy. BrdU detection was performed as described previously [34] with small modifications. Briefly, after permeabilization, cells were treated with 2 M HCl for 15 minutes at room temperature to expose the incorporated BrdU residues for indirect detection by antibody staining.

2.5. WGA-HRP-Labelling and In Vivo DAB-Cytochemistry

To label endocytic membranes in fibroblasts, pulse-chase labelling with wheat germ agglutinin coupled with horseradish peroxidase (WGA-HRP) was performed, following the protocol established by [32] adapted to HCMV-infected fibroblasts. Briefly, fibroblasts were cultured on carbon-coated sapphire discs (diameter: 3 mm, thickness: 160 µm, Engineering Offices M. Wohlwend GmbH, Switzerland) and infected with HCMV or left uninfected. On the day of high-pressure freezing, sapphire discs were transferred to an empty 6-well plate, while the culture medium was removed using filter paper. Subsequently, 10 µl of WGA-HRP solution (200 µg/ml) in fibroblast culture medium was directly placed onto each sapphire disc. For the control cells without WGA-HRP labelling but with DAB-H_2O_2 treatment, 10 µl of fibroblast culture medium was added instead. Samples were then incubated for 60 minutes at 37 °C with 5% CO_2 or for 10 minutes at 4 °C (pulse). Then, the WGA-HRP solution was removed from the sapphire discs using filter paper, and the discs were carefully placed into wells of a 6-well plate containing HEPES-buffered culture medium for 30 minutes at 37 °C with 5% CO_2 (chase). For the 4 °C control, this incubation step was performed at 4 °C. To induce the formation of the insoluble 3,3'-diaminobenzidine (DAB) reaction product, HEPES-buffered culture medium was replaced with a freshly prepared DAB solution (pH 7.0) containing 1.5 mg/ml DAB (Sigma-Aldrich GmbH, Germany), 70 mM NaCl (Merck KGaA, Germany), 50 mM ascorbic acid (VWR international, Germany), and 20 mM HEPES buffer. The addition of ascorbic acid as a non-membrane permeable antioxidant prevents the formation of insoluble DAB precipitate on the plasma membrane of the living cell and thus protects the cell from dying. After a 15 minutes pre-incubation at 4 °C in the dark, H_2O_2 (Merck KGaA, Germany) was added slowly and dropwise to the DAB solution, which gradually reached the final concentration of 0.025% H_2O_2, and incubated for another 30 minutes at 4 °C in the dark. For the control with WGA-HRP incubation but without the DAB-H_2O_2 reaction, cells were transferred to HEPES-buffered fibroblast culture medium without additives.

2.6. Sample Preparation for Electron Microscopy

Samples for electron microscopy were prepared as described in [35] with some modifications. After performing *in vivo* DAB-cytochemistry, samples were immediately cryo-immobilized in a Wohlwend HPF compact 01 high-pressure freezer (Engineering Office M. Wohlwend GmbH, Switzerland). Samples were subsequently freeze-substituted in a solution containing 1.0% (v/v) osmium tetroxide (ChemPur, Germany) and 0.1% uranyl acetate (w/v) (Merck KGaA, Germany) in acetone, supplemented with 5% (v/v) water to enhance membrane contrast [36]. Over a period of 17 hours, the temperature was gradually increased from −90 °C to 0 °C, with a one-hour incubation step at 0 °C and a further increase to room temperature within one hour. Samples were then rinsed three times with acetone, infiltrated incrementally with Epon 812 (30%, 60%, and 100% Epon in acetone), and finally polymerized at 60 °C for at least 48 hours. The sapphire discs were removed, leaving the cells and the carbon coat on the surface of the Epon block.

 doi:10.20944/preprints202408.1752.v1

2.7. Transmission Electron Microscopy and Quantification

For transmission electron microscopy (TEM), 70 nm sections were cut from the Epon block using an Ultracut UCT ultramicrotome (Leica, Germany) equipped with a 45° diamond knife (Diatome Ltd, Switzerland). Sections were collected on freshly glow-discharged single slot copper grids which were coated with a carbon-reinforced Formvar film. The sections were examined with a JEM-1400 transmission electron microscope (Jeol, Japan) operating at 120 kV acceleration voltage. Images were acquired using a Veleta CCD camera (Olympus, Japan). The grey value profile was measured for some of the budding and enveloped capsids using the Fiji analyze tool "Plot Profile" [37]. For quantification of capsids, images were acquired as described previously [38]: Only cVACs containing more than ten capsids were considered for quantification. Images were acquired with sufficient resolution to distinguish the different secondary envelopment stages and WGA labelling and covered the entire cVAC. Capsids were manually classified as either budding (WGA-positive or WGA-negative) or enveloped (WGA-positive or WGA-negative), counted using the JMicroVision v1.3.4 image analysis software [39], and the results were visualized in GraphPad 10.1.2. In the diagram the total number of budding and enveloped capsids per cell, respectively, was set to 100%.

2.8. Scanning Transmission Electron Microscopy Tomography

For three-dimensional (3D) visualization of the Golgi area and budding capsids, scanning transmission electron microscopy (STEM) tomography was performed. For that, samples were prepared as described previously [40]. In brief, 700 nm thick sections were cut from the Epon block using an Ultracut UCT ultramicrotome (Leica, Germany) equipped with a 35° diamond knife. Sections were then collected on freshly glow-discharged copper grids with parallel bars, which were pre-treated with a 10% (w/v) poly-L-lysine solution (Sigma-Aldrich GmbH, Germany) in water. After drying for 5 minutes at 37 °C, sections were immersed in a 1:2 diluted colloidal gold suspension as fiducial markers (Aurion, Netherlands) and coated with a 5 nm carbon layer (BAF 300, Balzers, Lichtenstein). STEM data were acquired with a JEM-2100F electron microscope (Jeol, Japan) operating at 200 kV acceleration voltage and equipped with a bright-field detector (EM-24541SIOD, Jeol, Japan). A tilt series of 97 STEM bright-field images was recorded from -72° to 72° at 1.5° increment. Tomograms were reconstructed using the IMOD software package version 4.7 [41] following the procedure described by [42] 3D visualizations and the video were generated with Avizo 3D 2020.2 (ThermoFisher Scientific Inc., USA) after manual segmentation.

3. Results

WGA labels the endocytic compartment. We applied WGA-HRP labelling and *in vivo* DAB-cytochemistry protocols together with high-pressure freezing and freeze substitution (HPF-FS) to identify the endocytic compartment in human fibroblasts by electron microscopy [32]. Fibroblasts were incubated with WGA-HRP for a 60 minutes pulse followed by a 30 minutes chase, both at 37 °C, to ensure saturation of the endocytic compartment and a sufficient labelling intensity. Subsequently, an *in vivo* DAB reaction was performed for 30 minutes at 4 °C to induce the formation of an electron-dense DAB precipitate.

TEM imaging of human fibroblasts labelled with WGA-HRP showed different intracellular membrane compartments with a luminal electron-dense layer, corresponding to the DAB precipitate (Figure 1A, arrowheads). Such DAB precipitates were not observed in control cells that were not labelled with WGA-HRP (Figure S1). Thus, internalization and intracellular distribution of WGA-HRP can be detected via these DAB precipitates. Consistent with previous findings [43], the DAB precipitate was frequently concentrated in vesicles of various sizes that were distributed throughout the cytoplasm and are presumably endosomes. In addition, multivesicular bodies (MVBs), appearing as large vesicles with small intraluminal vesicles, were WGA positive (Figure 1A, white asterisks). The WGA-positive endocytic compartment extended to the *trans*-side of the Golgi apparatus, with DAB precipitate confined either to the entire cross-section of the *trans*-most Golgi cisternae (Figure 1B, black asterisks) or to their terminal regions (Figure 1A, black asterisks). The observed labelling of *trans*-Golgi membranes by WGA is consistent with the retrograde transport of proteins and lipids

 doi:10.20944/preprints202408.1752.v1

from the plasma membrane via endosomes to the *trans*-Golgi network (TGN) [44,45]. These results confirm successful labelling and visualization of the endocytic compartment by WGA-HRP and TEM in human fibroblasts by the applied protocol.

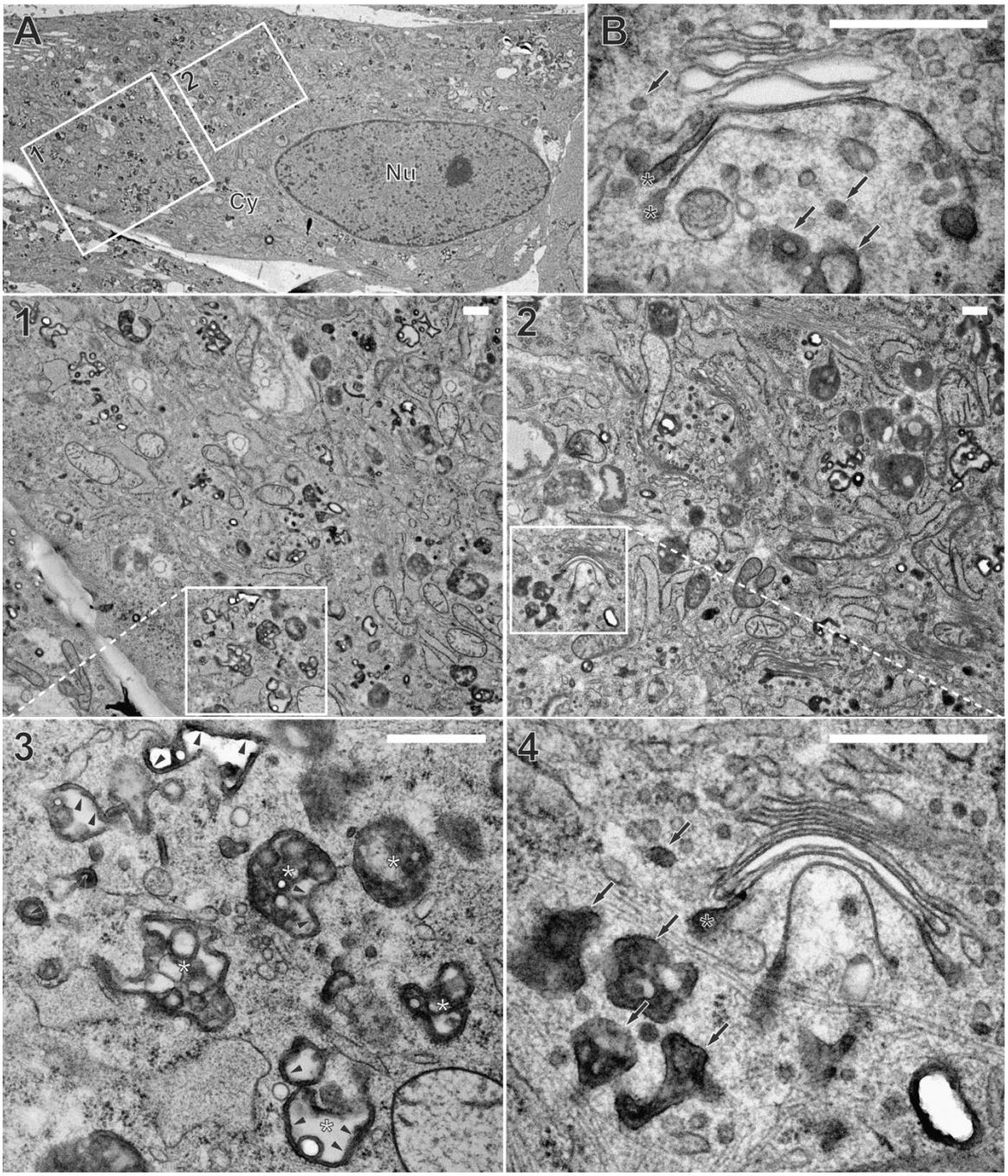

Figure 1. Non-infected fibroblasts, labelled with wheat germ agglutinin coupled to horse radish peroxidase (WGA-HRP) for 60 minutes pulse and 30 minutes chase, both at 37 °C. *In vivo* diaminobenzidine (DAB) cytochemistry was followed by high-pressure freezing, freeze substitution (HPF-FS) and Epon embedding. (A) Overview of a cell with corresponding details shown in panels 1-4. (1,2) DAB precipitate appears dark and labels WGA-positive membranes that are distributed throughout the cytoplasm. (3-4) Detailed depiction of DAB precipitate. Note its localization at the luminal face of intercellular membrane compartments (arrowheads). (3) Large WGA-positive endosomes are located close to the cell surface, often containing small intraluminal vesicles (=multivesicular bodies (MVBs), white asterisks). (4) Vesicles of the endocytic compartment with different sizes (arrows) can be found close to trans-Golgi membranes. WGA-positive membranes were also part of Golgi cisternae (black asterisks), either at the terminal regions of the trans-most Golgi

 doi:10.20944/preprints202408.1752.v1

cisternae or (B) decorating the entire cross section of the trans-most cisternae. Cy cytoplasm, Nu nucleus. Scale bars, 500 nm.

To verify the identity of the WGA-positive membrane compartments observed in TEM, fluorescently labelled WGA (WGA-FITC) was used to label human fibroblasts for 60 minutes followed by a 30 minutes chase, both at 37 °C, prior to fixation and indirect immunofluorescence staining for various cellular marker proteins.

WGA-FITC accumulated in vesicles of various sizes in the cytoplasm (Figure 2A). Most of these signals were perinuclear but also localized near the plasma membrane. Additionally, weaker WGA-FITC signals were observed on juxtanuclear membrane structures that exhibited a similar appearance to Golgi membranes, thereby corroborating the findings of the electron microscopy analysis. Counterstaining for cellular compartment marker proteins by using specific antibodies served to further identify the WGA-positive membrane compartments. EEA1 was used as a marker for early endosomes, CD63 as a marker for MVBs and late endosomes, GM130 as a marker for cis-Golgi membranes [4] and γ-Adaptin [46] (Figure 2B), Golgin97 [47] and TGN46 [48] as markers for the TGN (Figure S2). The vesicles that accumulated with WGA-FITC were positive for the early endosome marker EEA1 but negative for the MVB marker CD63 as well as negative for TGN and cis-Golgi-markers, confirming the internalization and enrichment of WGA in the early endosomal compartment in human fibroblasts. Together, these experiments demonstrate the rapid internalization and distribution of WGA into the endosomal compartment and its further dissemination to MVBs and *trans*-Golgi cisternae in non-infected human fibroblasts.

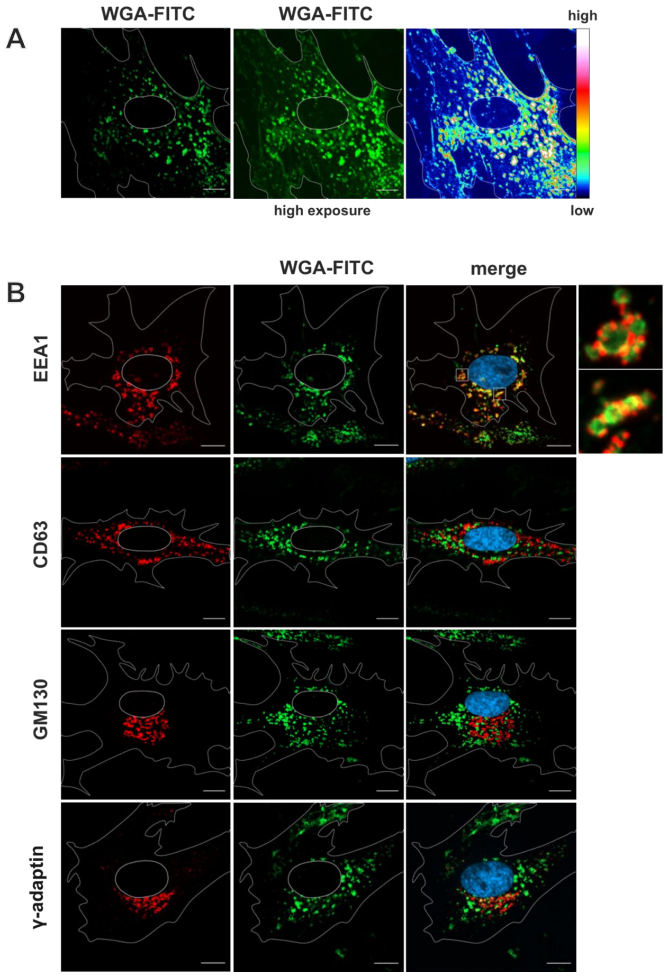

Figure 2. Immunofluorescence microscopy of fibroblasts labelled with WGA-FITC (10 µg/ml) with a 60 minutes pulse and 30 minutes chase, both at 37 °C. (A) WGA-FITC (green) strongly accumulates in cytoplasmic vesicles of various sizes. Weaker juxtanuclear signals resembling Golgi membranes are also visible. (B) Overlap of WGA-FITC signal with different cellular compartment markers (red).

 doi:10.20944/preprints202408.1752.v1

Higher magnification images of selected areas were recorded with longer exposure times to demonstrate the overlap of WGA-positive vesicular signals with EEA1-positive early endosomes. Scale bars, 10 μm.

Rapid accumulation of WGA at the cVAC together with nucleocapsids. HCMV infection causes significant changes to intracellular membrane systems, including the endocytic compartment [4,49]. This results in the formation of the cytoplasmic viral assembly complex (cVAC), where nascent virus particles acquire their lipid bilayer envelope through a budding process at intracellular membranes [50]. To investigate HCMV-induced changes in the endocytic compartment and to evaluate its role in cVAC biogenesis and virion maturation, we employed WGA-FITC labelling of HCMV-infected fibroblasts at 120 hpi using a 60 minutes pulse followed by a 30 minutes chase.

WGA-FITC accumulated as a diffuse signal in the region of the cVAC (Figure 3). This region is defined as the juxtanuclear cytoplasmic region positive for the viral tegument protein pUL99, delineated by a ring of *cis*-Golgi membranes positive for GM130 [7]. The diffuse WGA signals also overlapped with signals for the HCMV tegument protein pUL71 and glycoprotein gM (Figure S3). Both proteins are known to accumulate at the cVAC and to play important roles in virion morphogenesis [3,25,26]. In addition to the diffuse signals at the cVAC, WGA-FITC accumulated in vesicles of different sizes surrounding the cVAC. To determine whether the WGA signal at the cVAC resulted from endocytic uptake of WGA at the plasma membrane, WGA-labelling was performed under endocytosis-inhibiting conditions at 4 °C [51]. Under these conditions, WGA-FITC was not internalized and remained at the plasma membrane, indicating that accumulation of WGA at the cVAC requires endocytosis of labelled membranes. Together, these results show that a 60 minutes pulse followed by 30 minutes chase at 37 °C is sufficient to concentrate WGA at the cVAC. Furthermore, the difference in WGA distribution compared to non-infected human fibroblasts underscores the extensive re-organization of the cellular membrane systems by HCMV infection.

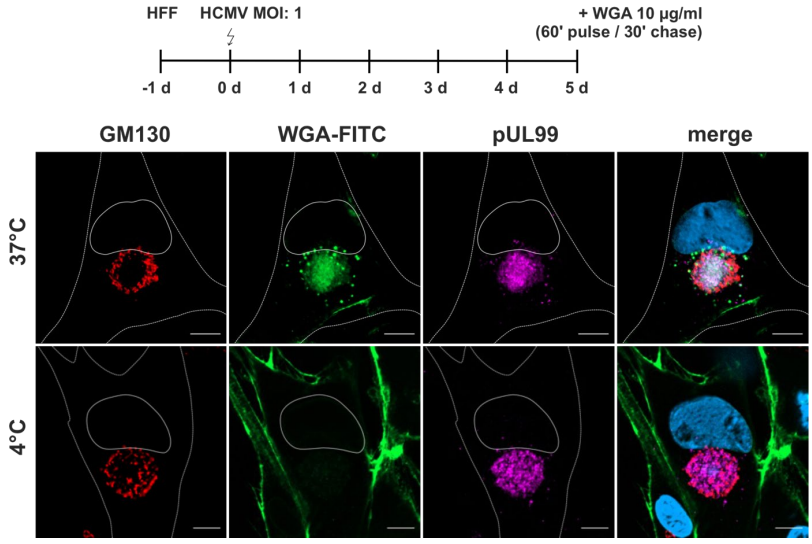

Figure 3. WGA internalization into HCMV-infected fibroblasts at 120 hpi. Fibroblasts were labelled with WGA-FITC (10 µg/ml) with a 60 minutes pulse and 30 minutes chase, both at either 37 °C or 4 °C. At 37 °C, WGA-FITC (green) is internalized and accumulates as a diffuse signal at the cVAC, which is marked by the viral protein pUL99 (magenta) and delimited by the *cis*-Golgi marker GM130 (red). In addition, WGA-FITC accumulates in vesicles of different sizes outside the cVAC. Internalization of WGA is inhibited at 4 °C, leading to its accumulation at the plasma membrane. Scale bars, 10 µm.

As for non-infected fibroblasts, we counterstained WGA-FITC-labelled fibroblasts for cellular organelle markers and examined the overlap of their signals with the signals for WGA-FITC (Figure 4A). Additional staining for HCMV pUL99 served as a marker for infected cells and to indicate the cVAC. EEA1-positive early endosomes were detected surrounding the cVAC and showed overlap with the punctate WGA-FITC signals outside the cVAC region, but not with the diffuse WGA-FITC

 doi:10.20944/preprints202408.1752.v1

signals within the cVAC. In contrast to previous data [4], we did not observe accumulation of EEA1 at the cVAC, suggesting that early endosomes were not enriched at the site of HCMV secondary envelopment in our experimental setup. CD63-positive membranes were also localized mainly outside the cVAC region. Surprisingly, some of the CD63-positive vesicles were also positive for WGA-FITC, however, most CD63-positive membranes surrounding the cVAC were negative for WGA-FITC. The partial overlap of WGA with CD63 was not observed in uninfected cells and is (again) an expression of viral manipulation of the cellular membrane systems. As expected, signals for γ-Adaptin and TGN46 were equally distributed within the cVAC [9,17,52], like pUL99, and exhibited substantial overlap with the diffuse WGA-FITC signals there. In contrast, the TGN-resident membrane marker Golgin97 was found in the peripheral region of the cVAC, thus showing only partial overlap with WGA-FITC at the cVAC.

This data shows a shift in the cellular distribution of WGA-positive membranes upon HCMV infection leading to their accumulation at the cVAC in a diffuse manner, similar to the TGN markers γ-Adaptin and TGN46. Furthermore, infection causes a shift of WGA-FITC distribution towards MVBs, as more overlap of WGA-FITC signals with those for CD63 is observed in infected than in non-infected fibroblasts (Figure 4).

Several studies have shown a concentration of recycling endosome markers at the cVAC, such as the transferrin receptor (TfR), Rab11, and Arf6, identifying recycling endosomes as an important structural component of the cVAC [25,53]. To investigate whether the WGA-positive endocytic compartment includes recycling endosomes, we labelled infected fibroblasts simultaneously with WGA-FITC and Transferrin conjugated with AlexaFluor555 (Tf-AF555) for a 60 minutes pulse followed by a 30 minutes chase. As shown in Figure 4B, Tf-AF555 accumulated together with WGA-FITC at the cVAC with a similar signal distribution although the WGA-FITC signals appeared slightly more diffuse. Consistent with the trafficking of WGA-FITC and TfR through early endosomes [54], several EEA1-positive vesicles surrounding the cVAC were also positive for WGA and Tf-AF555. These data identify recycling endosomes as a component of the endocytic compartment that can be identified by WGA and underscore the potential role of recycling endosomes for cVAC biogenesis and as the potential site of secondary envelopment of HCMV.

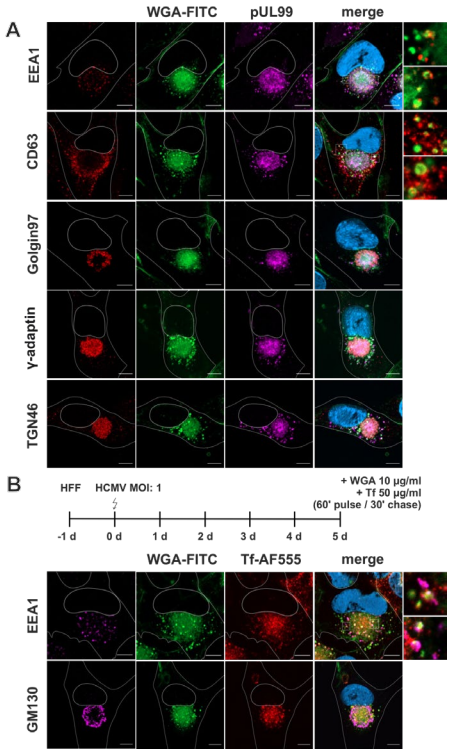

Figure 4. Characterization of the endocytic compartment in HCMV-infected fibroblasts. Higher magnification images were recorded with longer exposure time. Scale bars, 10 µm. (A) Screening of cellular compartment markers (red) in relation to WGA-FITC (green). Fibroblasts were labelled with

 doi:10.20944/preprints202408.1752.v1

WGA-FITC (10 µg/ml) with a 60 minutes pulse and 30 minutes chase, both at 37 °C. Higher magnifications show that the punctate WGA-FITC signals at the periphery of the cVAC overlap with EEA1-positive early endosomes and CD63-positive MVBs. The diffuse WGA-FITC signal within the cVAC appears similar to the ɣ-Adaptin and TGN46 signals. (B) Infected fibroblasts were simultaneously labelled with WGA-FITC (10 µg/ml) and Tf-AF555 (50 µg/ml) with a 60 minutes pulse and 30 minutes chase, both at 37 °C. WGA-FITC (green) and transferrin (Tf, red) localize at the cVAC in a similar pattern.

Secondary envelopment requires, in addition to host cell membranes, the presence of viral capsids at the cVAC. To identify nucleocapsids at the cVAC in relation to WGA-positive membranes, we performed BrdU labelling of viral genomes that became incorporated into capsids. The results show an accumulation of BrdU signals at the cVAC, representing nucleocapsids that were generated during the BrdU labelling period. Their signal overlapped with signals of WGA-FITC (Figure 5).

Thus, we could show that labelling of the endocytic compartment by WGA leads to a rapid accumulation of WGA at the cVAC with a distribution pattern like that of viral tegument and glycoproteins, and that the WGA-positive endocytic compartment includes membranes of recycling endosomes and the TGN. Furthermore, the accumulation of nucleocapsids at the WGA-positive region suggests that HCMV utilizes WGA-labelled endocytosed membranes for secondary envelopment.

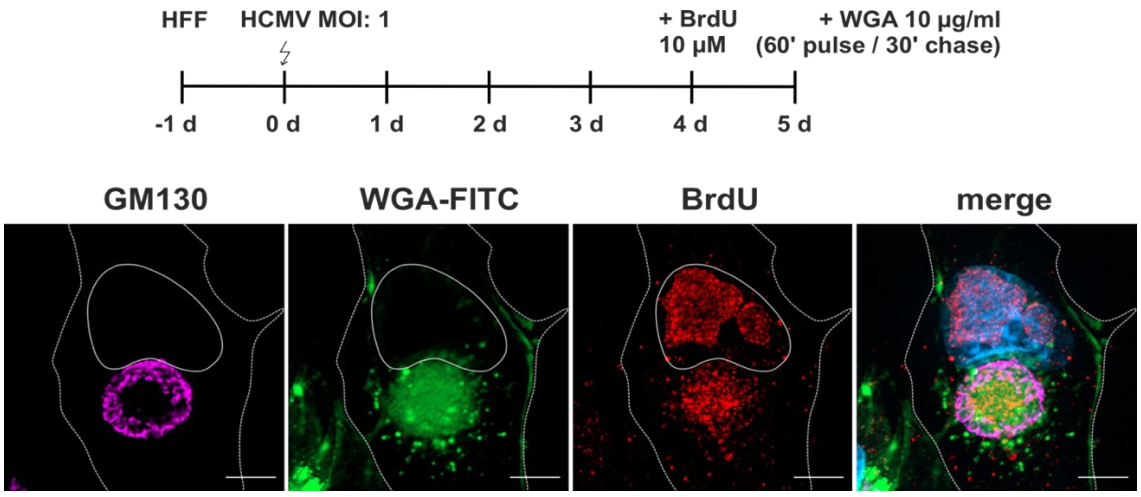

Figure 5. Localization of WGA relative to nucleocapsids. Infected fibroblasts were labelled with a 24 h pulse of BrdU (10 µM) at 96 hpi, followed by WGA-FITC labelling with a 60 minutes pulse and 30 minutes chase at 120 hpi, both at 37 °C. Labelling of viral DNA by BrdU (red) shows the juxtanuclear accumulation of HCMV nucleocapsids at similar regions as the diffuse WGA-FITC signal (green) at the cVAC, here delimited by the GM130 signal (magenta). Scale bars, 10 µm.

HCMV utilizes the endocytic compartment for secondary envelopment. To investigate the role of the endocytic compartment in HCMV secondary envelopment, we performed TEM after applying WGA-HRP labelling of HCMV-infected fibroblasts at 120 hpi. The cVACs exhibited conspicuous accumulations of DAB precipitates in the lumen of membranes, indicative for WGA-positive vesicles (Figure 6A and B). These signals were distributed over the entire cVAC region. Vesicles of different sizes and shapes, e.g. tubular and spherical, exhibited characteristic DAB precipitates (Figure 6B-E). Furthermore, some cisternae of the Golgi membrane stacks were repeatedly found to be WGA-positive, consistent with our observations in non-infected fibroblasts (Figure 6C). It should be noted that not all membranes within the cVAC region were WGA-positive (Figure 6C-D**)**. Importantly, other cellular membranes outside the cVAC, including those of mitochondria, the endoplasmic reticulum, and most Golgi stacks, were lacking DAB precipitates (Figure 6B) and DAB precipitates were absent in infected cells when WGA-HRP labelling was performed under endocytosis-inhibiting conditions at 4 °C (Figure S4) [51]. This verified the requirement of endocytosis for uptake of WGA into infected

 doi:10.20944/preprints202408.1752.v1

cells and confirmed the endocytic origin of the WGA-positive vesicles and the specificity of the WGA-labelling. In summary, it was shown that a large proportion of membranes in the cVAC region are provided by the endocytic compartment, thus representing a significant membrane source.

In the cVAC region, the various stages of virion maturation were identified, including *naked* capsids, capsids undergoing secondary envelopment (*budding* capsids), and *enveloped* capsids (Figure 6C-G). These stages are also typically found in infected cells that have not been subjected to the labelling procedure [38,50], demonstrating that WGA labelling has no apparent effect on virus morphogenesis. Many of the membranes on which budding was observed (Figure 6E and F, Figure 7A), as well as membranes of several enveloped capsids (Figure 6E and G), were WGA positive. This clearly shows that membranes of the endocytic compartment are used for secondary envelopment. In addition, as expected, there were also capsids lacking WGA on their membranes (Figure 6D).

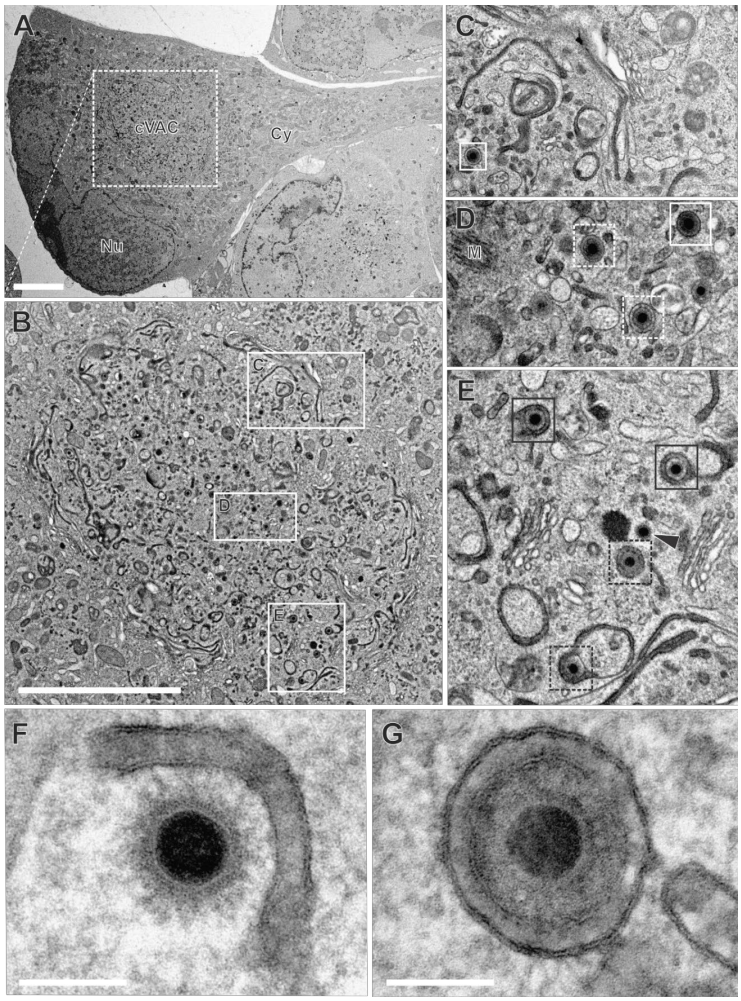

Figure 6. HCMV-infected fibroblasts, labelled with WGA-HRP, followed by *in vivo* DAB cytochemistry. (A) Overview. Nu nucleus, Cy cytoplasm, cVAC cytoplasmic viral assembly complex. (B) WGA-positive membrane compartments within the cVAC, including tubular and spherical vesicles (B-E) or stacked Golgi cisternae (C and E). (C-G) Capsids at various stages of secondary envelopment and their association with WGA-positive (black boxes) or WGA-negative (white boxes) vesicles. Enveloped capsids (solid boxes), budding capsids (dashed boxes), naked capsid (black arrowhead), M microtubule organizing center. (F) Capsid budding into a WGA-positive vesicle and (G) enveloped capsid within a WGA-positive vesicle. Quantitative results of this cell in Figure S5B "cell 7". Scale bars 5 μm (A, B), 100 nm (F, G).

Besides the secondary envelopment of capsids, the formation of dense bodies (DBs) could also be observed in TEM images (Figures 7B and D). DBs are characterized in EM as enveloped, electron-dense, homogeneous protein aggregates that are similar in size to virions. In contrast to virions,

 doi:10.20944/preprints202408.1752.v1

however, they contain neither a capsid nor an electron-dense DNA core. As for capsids (Figure 7A), the budding of such protein aggregates was observed at WGA-positive membranes (Figure 7B), suggesting a common envelopment mechanism for DBs and capsids. Moreover, the similarity of labelled and non-labelled membrane profiles (Figure 7) indicates no obvious impairment of the envelopment process due to WGA-HRP labelling.

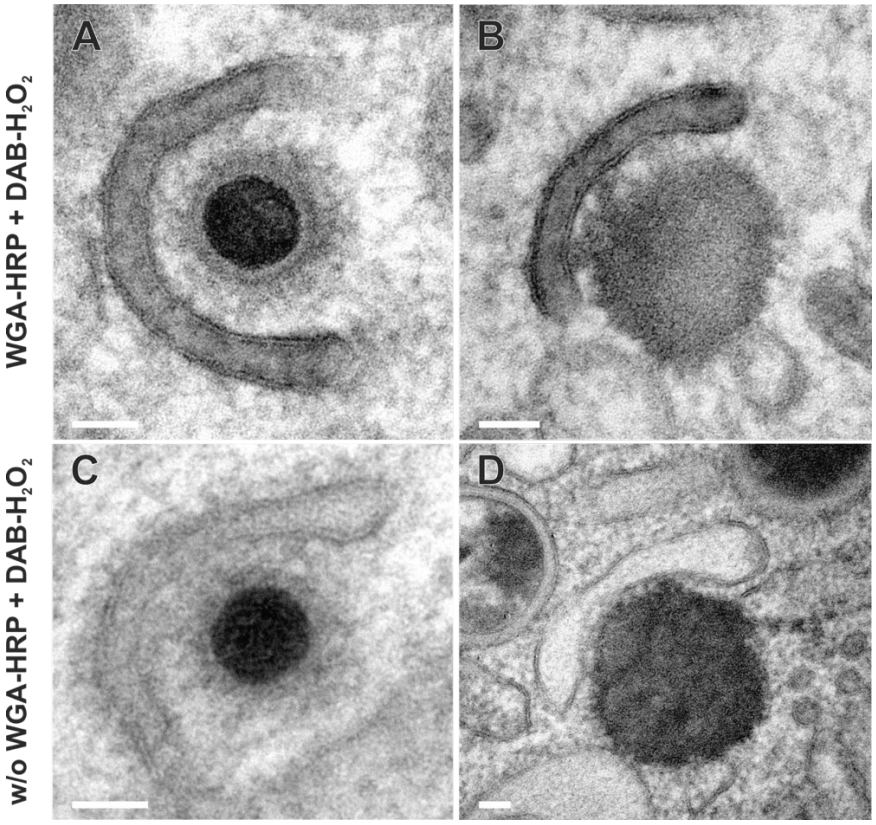

Figure 7. Capsid (A) and dense body (DB) (B) during secondary envelopment at WGA positive membranes, suggesting a common envelopment mechanism. Capsid (C) and DB (D) during secondary envelopment in control samples without WGA-HRP labelling. The membrane profiles show no obvious difference when the membranes were labelled with WGA-HRP. Scale bars, 50 nm.

Virion assembly at the cVAC is dynamic. To better understand the extent to which WGA-labelled membranes are involved in secondary envelopment, the different stages of envelopment of HCMV capsids were quantified from TEM images. For that, infected cells were randomly selected for quantification if they exhibited typical morphological features of late-stage infected cells, such as a kidney-shaped nucleus filled with numerous nuclear capsids and recognizable replication centers (Figure 6), accumulations of fragmented ER membranes in the cytoplasm outside the cVAC region [55], and the characteristic cVAC structure delineated by stacked Golgi-cisternae [38]. The capsids in the cVAC region were classified into four categories: 1a *labelled* (=WGA-positive) *budding* capsids, 1b *non-labelled* (=WGA-negative) *budding* capsids; 2a *labelled enveloped* capsids and 2b *non-labelled enveloped* capsids. Unclear virus capsids were classified as WGA-positive or WGA-negative based on a grey-value measurement of the space between the envelope and the vesicle membrane in comparison to the tegument (Figure S5). In the analysis of ten cells, 64.7% of all capsids were classified as budding capsids and 35.3% had completed secondary envelopment (Table 1). A similar ratio of budding versus enveloped capsids was found in cells that were not treated with WGA-HRP, again, confirming that WGA-HRP labelling had no adverse effects on secondary envelopment. When discriminating between budding events at WGA-positive and WGA-negative membranes, it was found that approximately 90% of all budding events occurred at WGA-positive vesicles (Table 1). This indicates that membranes originating from the plasma membrane reach the cVAC within 90 minutes and that secondary envelopment is initiated during this time. In addition, around 50% of the

 doi:10.20944/preprints202408.1752.v1

enveloped capsids were WGA positive, showing that secondary envelopment is not only initiated but also completed within 90 min. Although there were notable differences in the quantification across the 10 cells examined, all cells demonstrated that most capsids were associated with WGA-positive membranes (Figure S5B).

Together, our data demonstrate that secondary envelopment utilizes membranes of the endocytic compartment and indicate that secondary envelopment is a rapid process, highlighting the dynamic nature of HCMV assembly.

Table 1. Quantification of budding and enveloped capsids and their association with WGA-positive (WGA+) and WGA-negative (WGA-) membranes in human fibroblasts treated with WGA-HRP (60 minutes pulse, 30 minutes chase) followed by DAB and in cells not treated with WGA-HRP but with DAB only. Given are the mean percentages of budding and enveloped capsids per cVAC with standard deviation (SD), absolute numbers in brackets.

Sample	Membrane	Mean % ± SD (no. of capsids)	
		budding	enveloped
With WGA-HRP (423 capsids, 10 cells)		64.7% ± 9.5 (265)	35.3% ± 9.5 (158)
	WGA-pos.	**88.0%** ± 9.2 (227)	**48.8**% ± 19.0 (72)
	WGA-neg.	12.0% ± 9.2 (38)	51.2% ± 19.0 (86)
Without WGA-HRP (291 capsids, 9 cells)		63.2% ± 7.8 (183)	36.8% ± 7.8 (108)

To further narrow down the time frame in which secondary envelopment of HCMV is completed, we modified the labelling procedure. Labelling of late-stage infected fibroblasts was synchronized by their incubation with WGA-HRP at 4 °C for 10 min. The subsequent temperature shift to 37 °C for 30 minutes allowed the internalization of WGA-HRP into cells. Sufficient internalization and accumulation of WGA at the cVAC by the modified labelling procedure were confirmed using fluorescence microscopy and WGA-FITC (Figure S6).

In electron microscopy, numerous WGA-positive membranes were distributed throughout the cytoplasm of late-stage infected human fibroblasts (Figure 8B). Furthermore, we also observed budding of capsids at WGA-positive membranes (Figure 8C) and WGA-positive enveloped capsids (Figure 8D). This demonstrates extensive membrane dynamics and indicates that secondary envelopment is completed within a time frame of 30 minutes. However, as anticipated for a shorter labelling time, *budding* occurred more frequently at WGA-negative membranes (Figure 8E), and a greater number of WGA-negative *enveloped* capsids (Figure 8F) was observed in comparison to the experiments with a longer labelling time.

It is noteworthy that the shortening of the labelling pulse resulted in an altered labelling pattern within the cVAC, such that rather small vesicles were WGA-positive (Figure 8B). In addition, the Golgi region exhibited reduced and often less obvious WGA-labelling. Compared to the longer labelling time, only one or two of the *trans*-most Golgi cisternae were visibly WGA-positive. The staining in those cisternae was limited to the terminal regions and/or appeared as a striped pattern of DAB precipitate (Figure 8G and H). This striped pattern was also observed on HCMV envelopes (Figure 8G insert) and may indicate an association of WGA at certain parts of the plasma membrane. Furthermore, MVBs (Figure 8I) and vesicles in the *trans*-Golgi region were WGA-positive (Figure 8G), confirming the internalization and distribution of WGA along the endocytic pathway as previously reported [56].

 doi:10.20944/preprints202408.1752.v1

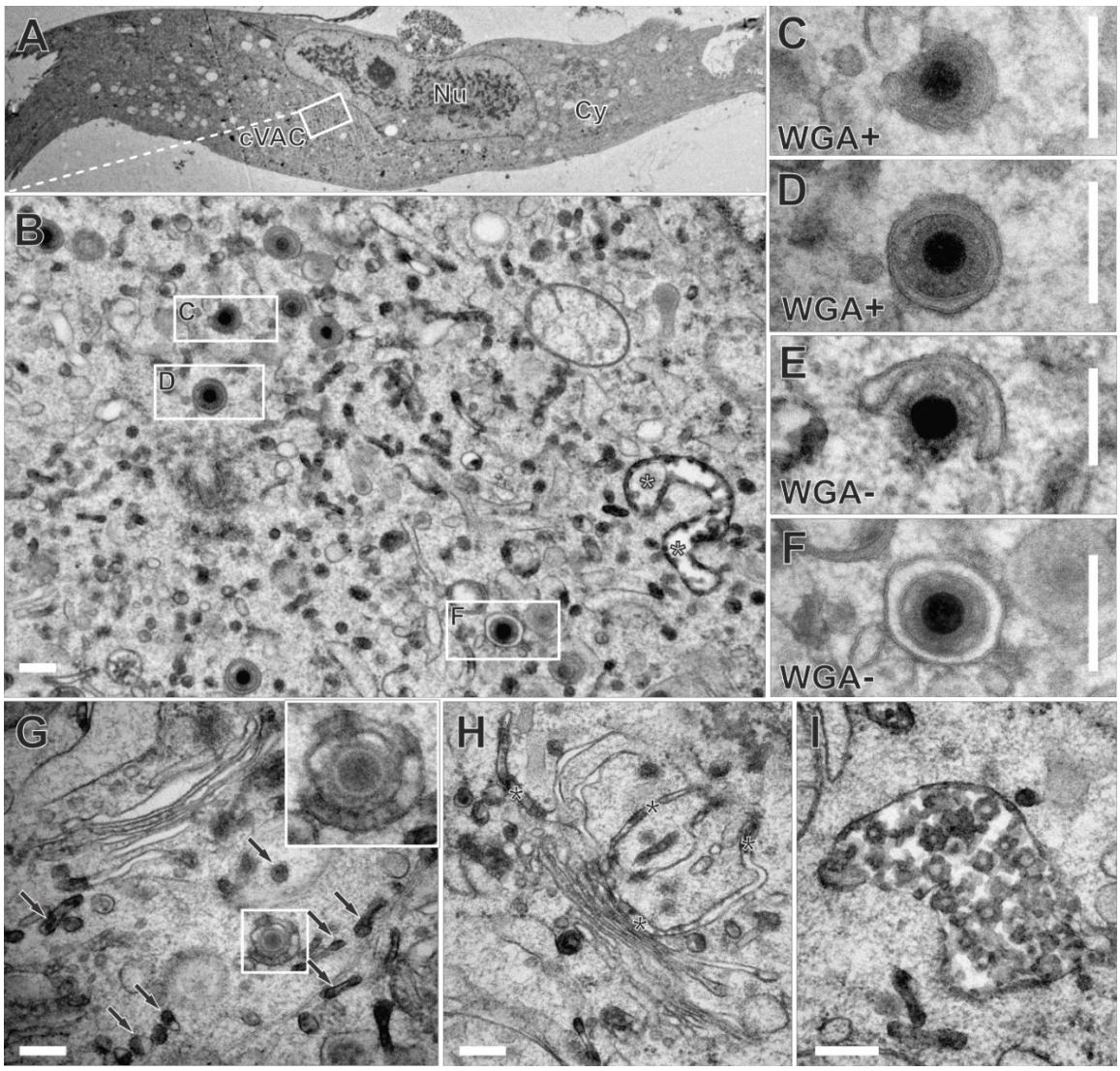

Figure 8. Infected fibroblast incubated with WGA-HRP for 10 minutes pulse at 4 °C and 30 minutes chase at 37 °C followed by *in vivo* DAB cytochemistry. (A) Overview. Nu nucleus, Cy cytoplasm, cVAC cytoplasmic viral assembly complex. (B) A region of the cVAC with WGA-positive large endosomes (white asterisks), and capsids. (C) Capsid budding at or (D) capsid enveloped in WGA-positive membrane. (E) Capsid budding at or (F) enveloped in WGA-negative membrane. (G) The *trans*-site of the Golgi apparatus is occupied by multiple WGA-positive vesicles (arrows). Note the budding event at the vesicle with a striped pattern of DAB precipitate (inset). (H) *Trans*-most stacked Golgi cisternae also exhibit a striped pattern of DAB precipitate (black asterisks). (I) MVB is filled with numerous WGA-positive intraluminal vesicles. Scale bars, 200 nm.

Role of the Golgi-apparatus and the endocytic *trans*-Golgi network in cVAC formation and secondary envelopment. It was observed in our experiments that the WGA-positive endocytic compartment in HCMV-infected fibroblasts also included Golgi cisternae. We also found that the *trans*-side of some of those Golgi stacks contained enveloped capsids (Figure 9). This suggested that the *trans*-sided membranes of the Golgi stacks can be utilized for secondary envelopment.

 doi:10.20944/preprints202408.1752.v1

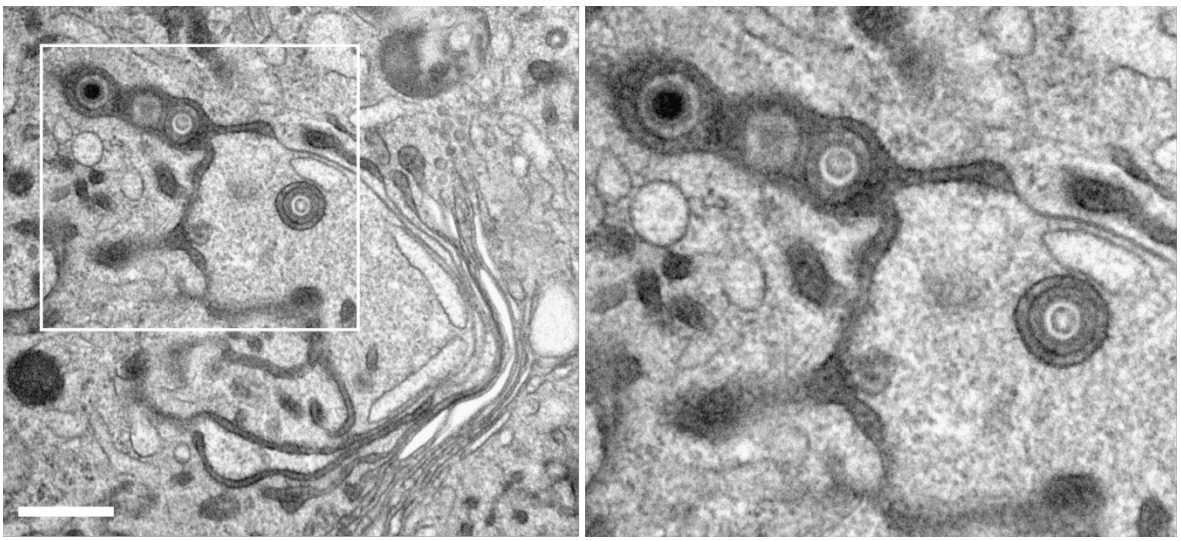

Figure 9. Capsids associated with WGA-positive Golgi membranes. Cells were labelled with WGA-HRP for 60 minutes pulse and 30 minutes chase, followed by *in vivo* DAB cytochemistry. Note the WGA-positive membranes at terminal regions of the *trans*-sided Golgi cisternae. Scale bar, 500 nm.

To examine the structural dependencies between the endocytic compartment, the TGN, and the stacked Golgi cisternae, and to identify their role in HCMV secondary envelopment and cVAC structure, we performed three-dimensional (3D) EM imaging. By using tomography, we can unambiguously determine whether there is an association of capsids with membranes of the *trans*-side of Golgi stacks and thus confirm secondary envelopment at Golgi membranes.

The tomogram shows an area of the cVAC that contains the TGN, a Golgi stack, and capsids and dense bodies at different stages of secondary envelopment (Figure 10). In 3D, the endocytic TGN (Figure 10A) appears as a large, reticulated structure, similar to what has been described for uninfected cells [56]. The *cis*-side of the Golgi stack faces the nucleus and the *trans*-side faces the cVAC. Numerous small vesicles, presumably Golgi vesicles, surround the Golgi stack. Several enveloped and budding capsids at membranes not connected to Golgi cisternae are shown. Most interestingly, we found capsids in the process of secondary envelopment at membranes of the *trans*-most Golgi cisterna (Figure 10 B and D; membrane profile visible in C and E). The lumen of these Golgi cisternae shows the characteristic staining for WGA-positive membranes, demonstrating its connection to the endocytic compartment. Taken together, our data demonstrate that HCMV utilizes membranes of stacked Golgi cisternae for secondary envelopment and that these membranes are also part of the endocytic compartment.

 doi:10.20944/preprints202408.1752.v1

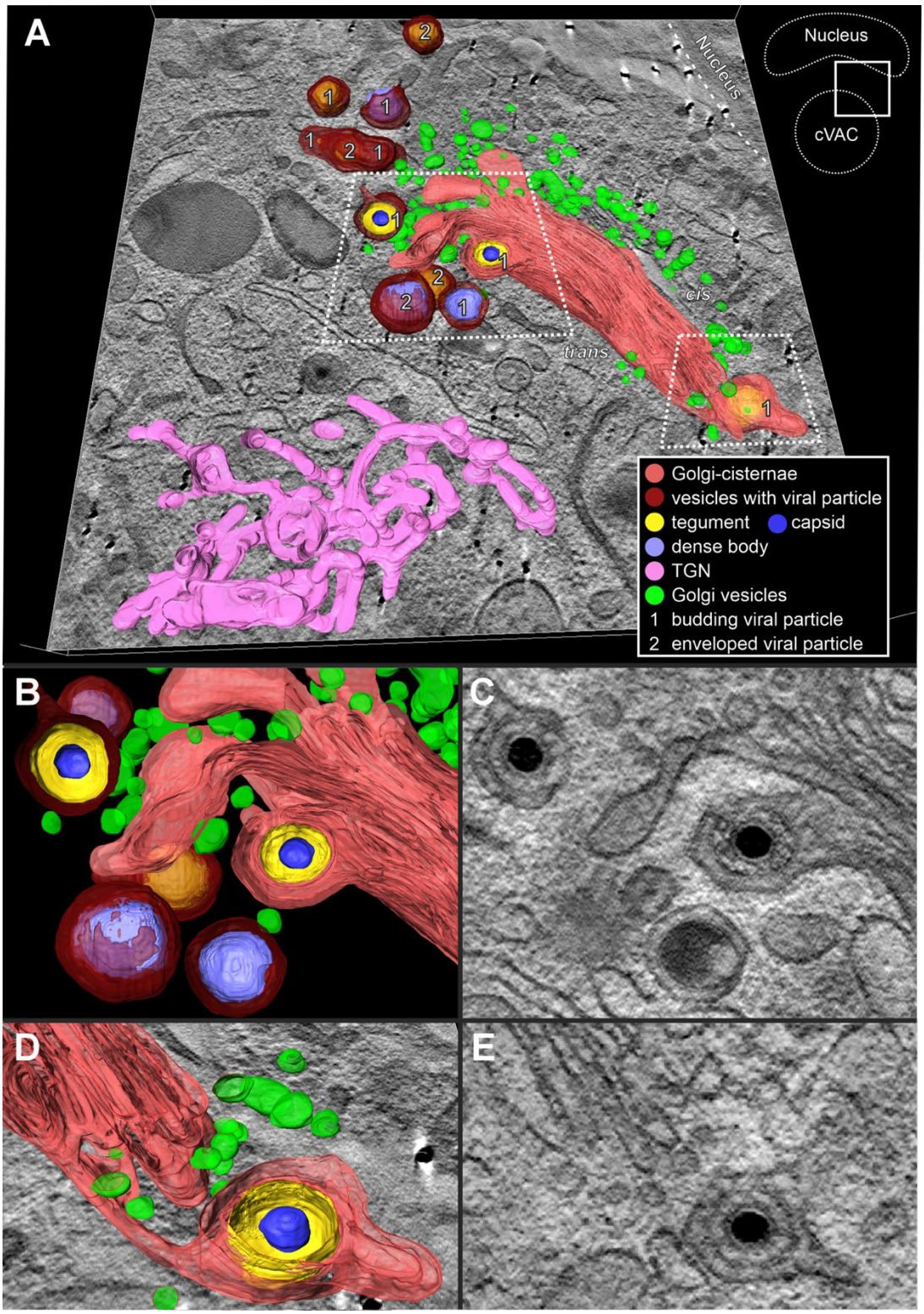

Figure 10. Three-dimensional (3D) visualization of the Golgi region in an HCMV-infected fibroblast from 150 virtual tomogram sections (each 3 nm thick). (A) Stacked Golgi cisternae with the *cis*-side facing the nucleus and the *trans*-side facing the cVAC. Capsids and DBs budding into or enveloped by membranes that are not connected to the Golgi cisternae (dark red) and capsids budding into Golgi cisternae were observed. (B-E) Capsids budding at the membrane of the *trans*-most Golgi cisterna. (D and E) The connection of the budding capsid with the Golgi stack could only be visualized by 3D EM. Video of this dataset in Supplementary Movie 1.

4. Discussion

 doi:10.20944/preprints202408.1752.v1

The general steps of the secondary envelopment of nucleocapsids are similar for all herpesviruses and well understood. Secondary envelopment begins with the binding of partially tegumented nucleocapsids to membranes in the cytoplasm. These contain viral glycoproteins and glycoprotein complexes as well as membrane-associated tegument proteins. The binding of the nucleocapsids to these membranes induces membrane curvature, whereby the membrane wraps around the capsid. The envelopment process is completed by membrane fission, resulting in mature virions located in cytoplasmic vesicles. Although secondary envelopment is an essential process for the formation of infectious viral progeny, little is known about its timing, especially in HCMV morphogenesis. By using WGA to label glycoproteins on the plasma membrane we were able to narrow down the time frame of secondary envelopment for the first time. In pulse-chase experiments in which we induced the endocytic uptake of WGA into the cell by a temperature shift to 37 °C for 30 minutes after binding of WGA to glycoproteins on the plasma membrane, we were able to find budding of nucleocapsids on WGA-positive membranes as well as already enveloped virions in WGA-positive vesicles in the cVAC (Figure 8). This shows that within this time, WGA-labelled glycoproteins are endocytosed and transported from the plasma membrane to the cVAC, where they are recognized by nucleocapsids, and secondary envelopment is initiated and also completed. This indicates that the actual time for the secondary envelopment process must be much shorter than 30 min. And it could also explain why only a few budding capsids are visible in infected cells while the majority of capsids is already enveloped [50]. Furthermore, our data suggest that HCMV has evolved mechanisms that enable the rapid transport of viral glycoproteins from the plasma membrane to the cVAC and a highly efficient strategy that allows nucleocapsids to recognize the membranes containing the required protein composition for the initiation and execution of secondary envelopment.

Similar studies on HSV-1 using HRP as a fluid phase endocytosis marker have shown that secondary envelopment can be detected at HRP-positive endosomes as early as two minutes after the addition of HRP, and that almost 90% of all capsids were found on HRP-positive membranes with a longer pulse of 30 minutes [23]. This is similar to our data, confirming that the processes leading to the secondary envelopment of herpesviruses are highly dynamic, but it also indicates that the actual envelopment process of HSV-1 is even more rapid. However, there are some differences between the HSV-1 study and our study that must be considered when comparing the results. Different methodological approaches were used to label the endocytic compartment (fluid phase HRP for HSV-1 versus WGA-HRP in this study). It should also be noted that HSV-1 has a much faster replication cycle than HCMV. In addition, HSV-1 does not establish a cVAC in which the secondary envelopment process takes place, except in certain neuronal cells (White and Roller 2024). However, what both approaches have in common is that the temporal limitation depends on additional processes, such as membrane dynamics, nucleocapsid formation, and intracellular transport of membranes and nucleocapsids to the site of secondary envelopment, which may also be virus and cell-type-dependent.

The cVAC is a highly specialized and dynamic cytoplasmic compartment established by betaherpesviruses [8,9,57]. The cVAC forms around the centrosome, which functions as a microtubule organizing center (MTOC) [2]. In addition, the cVAC itself serves as an MTOC, as HCMV infection induces a switch from centrosomal to non-centrosomal microtubules, which originate at the cis-Golgi membranes of the cVAC [9]. Viral manipulation of the microtubule cytoskeleton is not only crucial for the formation and maintenance of the cVAC [2,9] but is also important for optimized cargo import and export, thus contributing to the highly dynamic envelopment processes during HCMV virion morphogenesis. We show by electron microscopy that a large fraction of the cVAC membranes is WGA-positive after a 60 minutes pulse followed by a 30 minutes chase and thus indicate that membranes of the endocytic compartment accumulate at the site of secondary envelopment (Figure 6). Ultrastructural analysis could identify some of these membranes as MVBs and Golgi stacks, whereas for the latter only the *trans*-most cisternae were positive for WGA. A reticular structure positive for WGA, probably formed by the endocytic TGN [56], was also identified as part of the cVAC (Figure 10). However, other WGA-positive membranes at the cVAC, especially those serving

 doi:10.20944/preprints202408.1752.v1

nucleocapsids for budding, could not be unambiguously identified. Also, counterstaining with various cellular marker proteins, including EEA1 for early endosomes [4], CD63 for late endosomes and MVBs, and Golgi markers, did not result in exact colocalization with the endocytic, WGA-positive compartment (Figure 4). The most similar localization of WGA signals within the pUL99-positive center of the cVAC was found for the *trans*-Golgi markers γ-Adaptin and TGN46, and the recycling endosome marker TfR, whereas EEA1-positive early endosomes and late endosomes/MVBs tended to accumulate outside the *cis*-Golgi signals that mark the boundary of the cVAC. These results and the data from other groups confirm that there is no clear cellular marker for the membranes of the cVAC, especially not for the membranes involved in secondary envelopment. One explanation is that HCMV infection causes extensive changes in membrane compartments and membrane identities [4,49], which is also associated with the manipulation of host cell intracellular transport pathways, including the secretory and endocytic pathway [58,59]. All data to date suggest that HCMV generates the most suitable membrane composition to promote productive infection. This is emphasized by our fluorescence microscopy experiments showing a different distribution of CD63 and WGA in infected fibroblasts compared to uninfected fibroblasts. While WGA did not colocalize with CD63 in uninfected fibroblasts (Figure 2B), some of the CD63-positive vesicles in HCMV-infected fibroblasts were also positive for WGA (Figure 4A).

In this work, we show that HCMV nucleocapsids utilize different membranes in the cVAC for secondary envelopment. In addition to budding of nucleocapsids into endocytic vesicles and tubules of various sizes, budding was also found at membranes of Golgi cisternae (Figure 9 and 10). Interestingly, most of these membranes were positive for WGA after a 60 minutes pulse followed by a 30 minutes chase, which implies that glycoproteins previously labelled with WGA at the cell surface were retrieved from the plasma membrane and accumulated in these membranes. This was also the case for the Golgi cisternae, at which secondary envelopment was detected. Thus, the presence of viral glycoproteins appears to be an important aspect of the interaction of nucleocapsids with cellular membranes for the initiation of secondary envelopment. As in previous studies, no specific cellular compartment marker or membrane compartment used by HCMV for secondary envelopment could be identified. On the contrary, the observed budding into different membranes, the majority of which were WGA-positive, agrees with all previously postulated models regarding the membrane source of the viral envelope in HCMV infection [15–17] and provide an explanation for the different models. In our experiments, the most common feature of a membrane used for secondary envelopment was that it was a membrane enriched with glycoproteins that had previously been labelled with WGA on the plasma membrane. WGA-labelled glycoproteins are then distributed through the endocytic compartment and reach other cellular membranes, such as the TGN and *trans*-sided cis-Golgi cisternae. Although it is important to note that WGA labels both, cellular and viral glycoproteins, it is reasonable to assume that a significant proportion of the glycoproteins at the plasma membrane in the late stage of infection are of viral origin. Supporting this, viral glycoproteins are visible in TEM images as patches on the virion envelope [38]. In TEM images of WGA-labelled samples it appeared that the DAB precipitate accumulates preferentially at those patches, forming a striped WGA pattern on the virion envelope (Figure 8G). This model of glycoprotein distribution in HCMV-infected cells is further supported by the presence of endocytic trafficking motifs in the cytoplasmic domain of several viral glycoproteins, such as gB and gM, which play an important role in the localization and accumulation of these proteins at the cVAC. Furthermore, a similar trafficking pathway has already been demonstrated for the membrane-associated tegument protein pUL71 by the characterization of its endocytosis motifs [26].

We also found mature virions in WGA-negative membranes at the cVAC, and also budding at such membranes (Figure 6 and Table 1). We can only speculate about the identity of these membranes. One possible explanation is that these membranes predate the onset of WGA labelling and have not yet been replaced by WGA-labelled membranes. Alternatively, it is also possible that these are membranes originating from other routes and sources or from the chase period. Even if the latter cannot be completely excluded, in fluorescence labelling a chase of 30 minutes was not sufficient to purge the plasma membrane of all WGA signals. Future experiments with modified labelling

 doi:10.20944/preprints202408.1752.v1

procedures should be able to clarify this. As this example shows, dynamic processes cannot be directly visualized with EM, as in the end only snapshots of dynamic events are analyzed. However, with the help of pulse-chase experiments, as performed in this study, we can obtain indirect evidence of the dynamics of the processes investigated here. By this, we were able to get an insight into the dynamics of HCMV morphogenesis. In quantification experiments with a 60 minutes pulse followed by a 30 minutes chase, 50% of the capsids that completed envelopment were WGA-positive (Table 1). This is a remarkably high number considering that at the beginning of the WGA pulse, none of the enveloped capsids in the cVAC are positive for WGA and that several thousand capsids can be present at the cVAC at 120 hpi [50]. Even more remarkable is the finding that about 90% of budding events occurred at WGA-positive membranes. The higher ratio of budding capsids at WGA-positive membranes was expected since budding chronologically precedes full envelopment. Overall, our quantifications indicate that virus particles and membranes in the cVAC are subject to a high turnover and that the WGA-positive compartment at the cVAC is the main membrane source for secondary envelopment of HCMV capsids. It can be assumed that WGA-positive mature virions have already been released from the cells in our labelling experiments. However, due to the methodological procedure of *in vivo* DAB cytochemistry that requires ascorbic acid in the DAB reaction [32], WGA-positive envelopes cannot be visualized for extracellular virions. Therefore, we can only speculate about the release of labelled virions from the cells.

The labelling of (viral) glycoproteins at the plasma membrane by WGA led to a labelling of the endocytic compartment. To better understand which membranes are involved in secondary envelopment, future studies could specifically label viral glycoproteins or membrane-associated tegument proteins that have already been shown to be involved in secondary envelopment. This could be done through encodable HRP [60–62]. Furthermore, more specific labelling of distinct membrane compartments, such as recycling endosomes, could be achieved by using gold-coupled transferrin.

In this study, we combined fluorescence microscopy with advanced electron microscopy techniques to investigate the secondary envelopment of HCMV. Taken together, the direct and detailed visualization of capsids in the different stages of secondary envelopment and the high temporal resolution provided by high-pressure freezing, combined with the labelling of the endocytic compartment, revealed that endocytosed membranes are the major source for the cVAC membranes and for the HCMV envelope, which is acquired in a rapid process.

Supplementary Materials: The following supporting information can be downloaded at: www.mdpi.com/xxx/s1, Supplementary Movie 1: 3D visualization of the Golgi region of an HCMV-infected fibroblast; Figure S1: Non-infected fibroblast not labelled with WGA-HRP but treated with DAB and H_2O_2; Figure S2: Colocalization study of TGN protein markers and WGA-FITC in non-infected fibroblasts after 60 minutes pulse and 30 minutes chase; Figure S3: Immunofluorescence microscopy of cVAC associated viral proteins pUL71 and gM and WGA-FITC in HCMV-infected fibroblasts; Figure S4: Non-infected and HCMV-infected fibroblasts, incubated with WGA-HRP for a 60 minutes pulse and 30 minutes chase, both at 4 °C, and subjected to *in vivo* DAB cytochemistry; Figure S5: Grey value profiles of enveloped capsids after treatment with WGA-HRP but without DAB-H_2O_2 or treated with WGA-HRP and DAB-H2O2 or treated without WGA-HRP but with DAB-H_2O_2. Illustration of Data from Table 1; Figure S6: Internalization of WGA-FITC in HCMV-infected fibroblasts at 120 hpi after shorter labelling times.

Author Contributions: Conceptualization, T.B., J.v.E., and C.R.; methodology, T.B., G.F., L.C; formal analysis, T.B., L.C.; resources, C.R and J.v.E.; writing—original draft preparation, T.B., G.F., C.R., J.v.E.; writing—review and editing, T.B., L.C., G.F., C.R, J.v.E.; visualization, T.B., L.C.; supervision, C.R and J.v.E.; project administration, C.R and J.v.E.; funding acquisition, C.R. All authors have read and agreed to the published version of the manuscript.

Funding: This research was funded by a Collaborative Research Centre grant of the Deutsche Forschungsgemeinschaft (316249678 – SFB 1279) and by the Baden-Württemberg Stiftung (Project- ID MET-ID12-ABEM) to C.R.

Data Availability Statement: No further data is available.

 doi:10.20944/preprints202408.1752.v1

Acknowledgments: The authors would like to acknowledge the members of the Central Facility for Electron Microscopy, Ulm University, for technical support.

Conflicts of Interest: The authors declare no conflict of interest.

References

1. Das, S.; Vasanji, A.; Pellett, P.E. Three-Dimensional Structure of the Human Cytomegalovirus Cytoplasmic Virion Assembly Complex Includes a Reoriented Secretory Apparatus. *J Virol* **2007**, *81*, 11861–11869, doi:10.1128/JVI.01077-07.
2. Sanchez, V.; Greis, K.D.; Sztul, E.; Britt, W.J. Accumulation of Virion Tegument and Envelope Proteins in a Stable Cytoplasmic Compartment during Human Cytomegalovirus Replication: Characterization of a Potential Site of Virus Assembly. *J Virol* **2000**, *74*, 975–986, doi:10.1128/JVI.74.2.975-986.2000.
3. Schauflinger, M.; Fischer, D.; Schreiber, A.; Chevillotte, M.; Walther, P.; Mertens, T.; von Einem, J. The Tegument Protein UL71 of Human Cytomegalovirus Is Involved in Late Envelopment and Affects Multivesicular Bodies ▿. *J Virol* **2011**, *85*, 3821–3832, doi:10.1128/JVI.01540-10.
4. Das, S.; Pellett, P.E. Spatial Relationships between Markers for Secretory and Endosomal Machinery in Human Cytomegalovirus-Infected Cells versus Those in Uninfected Cells. *J Virol* **2011**, *85*, 5864–5879, doi:10.1128/JVI.00155-11.
5. Fraile-Ramos, A.; Kledal, T.N.; Pelchen-Matthews, A.; Bowers, K.; Schwartz, T.W.; Marsh, M. The Human Cytomegalovirus US28 Protein Is Located in Endocytic Vesicles and Undergoes Constitutive Endocytosis and Recycling. *Mol Biol Cell* **2001**, *12*, 1737–1749, doi:10.1091/mbc.12.6.1737.
6. Fraile-Ramos, A.; Pelchen-Matthews, A.; Kledal, T.N.; Browne, H.; Schwartz, T.W.; Marsh, M. Localization of HCMV UL33 and US27 in Endocytic Compartments and Viral Membranes. *Traffic* **2002**, *3*, 218–232, doi:10.1034/j.1600-0854.2002.030307.x.
7. Das, S.; Ortiz, D.A.; Gurczynski, S.J.; Khan, F.; Pellett, P.E. Identification of Human Cytomegalovirus Genes Important for Biogenesis of the Cytoplasmic Virion Assembly Complex. *J Virol* **2014**, *88*, 9086–9099, doi:10.1128/JVI.01141-14.
8. Lučin, P.; Jug Vučko, N.; Karleuša, L.; Mahmutefendić Lučin, H.; Blagojević Zagorac, G.; Lisnić, B.; Pavišić, V.; Marcelić, M.; Grabušić, K.; Brizić, I.; et al. Cytomegalovirus Generates Assembly Compartment in the Early Phase of Infection by Perturbation of Host-Cell Factors Recruitment at the Early Endosome/Endosomal Recycling Compartment/Trans-Golgi Interface. *Front Cell Dev Biol* **2020**, *8*, 563607, doi:10.3389/fcell.2020.563607.
9. Procter, D.J.; Banerjee, A.; Nukui, M.; Kruse, K.; Gaponenko, V.; Murphy, E.A.; Komarova, Y.; Walsh, D. The HCMV Assembly Compartment Is a Dynamic Golgi-Derived MTOC That Controls Nuclear Rotation and Virus Spread. *Dev Cell* **2018**, *45*, 83-100.e7, doi:10.1016/j.devcel.2018.03.010.
10. Wofford, A.S.; McCusker, I.; Green, J.C.; Vensko, T.A.; Pellett, P.E. Chapter Ten - Betaherpesvirus Assembly and Egress: Recent Advances Illuminate the Path. In *Advances in Virus Research*; Kielian, M., Mettenleiter, T.C., Roossinck, M.J., Eds.; Virus Assembly and Exit Pathways; Academic Press, 2020; Vol. 108, pp. 337–392.
11. Cruz, L.; Streck, N.T.; Ferguson, K.; Desai, T.; Desai, D.H.; Amin, S.G.; Buchkovich, N.J. Potent Inhibition of Human Cytomegalovirus by Modulation of Cellular SNARE Syntaxin 5. *Journal of Virology* **2016**, *91*, 10.1128/jvi.01637-16, doi:10.1128/jvi.01637-16.
12. Varnum, S.M.; Streblow, D.N.; Monroe, M.E.; Smith, P.; Auberry, K.J.; Pasa-Tolic, L.; Wang, D.; Camp, D.G.; Rodland, K.; Wiley, S.; et al. Identification of Proteins in Human Cytomegalovirus (HCMV) Particles: The HCMV Proteome. *J Virol* **2004**, *78*, 10960–10966, doi:10.1128/JVI.78.20.10960-10966.2004.
13. Liu, F.; Zhou, Z.H. Comparative Virion Structures of Human Herpesviruses. In *Human Herpesviruses: Biology, Therapy, and Immunoprophylaxis*; Arvin, A., Campadelli-Fiume, G., Mocarski, E., Moore, P.S., Roizman, B., Whitley, R., Yamanishi, K., Eds.; Cambridge University Press: Cambridge, 2007 ISBN 978-0-521-82714-0.
14. Kalejta, R.F. Tegument Proteins of Human Cytomegalovirus. *Microbiol Mol Biol Rev* **2008**, *72*, 249–265, doi:10.1128/MMBR.00040-07.
15. Tooze, J.; Hollinshead, M.; Reis, Burkhardt; Radsak, Klaus; Kern, Horst Progeny Vaccinia and Human Cytomegalovirus Particles Utilize Early Endosomal Cisternae for Their Envelopes. *Eur J Cell Biol.* **1993**.
16. Homman-Loudiyi, M.; Hultenby, K.; Britt, W.; Soderberg-Naucler, C. Envelopment of Human Cytomegalovirus Occurs by Budding into Golgi-Derived Vacuole Compartments Positive for gB, Rab 3, Trans-Golgi Network 46, and Mannosidase II. **2003**, *77*, doi:10.1128/jvi.77.5.3191-3203.2003pert.
17. Cepeda, V.; Esteban, M.; Fraile-Ramos, A. Human Cytomegalovirus Final Envelopment on Membranes Containing Both *Trans* -Golgi Network and Endosomal Markers. *Cellular Microbiology* **2010**, *12*, 386–404, doi:10.1111/j.1462-5822.2009.01405.x.

18. Gershon, A.A.; Sherman, D.L.; Zhu, Z.; Gabel, C.A.; Ambron, R.T.; Gershon, M.D. Intracellular Transport of Newly Synthesized Varicella-Zoster Virus: Final Envelopment in the Trans-Golgi Network. *J Virol* **1994**, *68*, 6372–6390, doi:10.1128/JVI.68.10.6372-6390.
19. Granzow, H.; Weiland, F.; Jöns, A.; Klupp, B.G.; Karger, A.; Mettenleiter, T.C. Ultrastructural Analysis of the Replication Cycle of Pseudorabies Virus in Cell Culture: A Reassessment. *J Virol* **1997**, *71*, 2072–2082, doi:10.1128/JVI.71.3.2072-2082.
20. McMillan, T.N.; Johnson, D.C. Cytoplasmic Domain of Herpes Simplex Virus gE Causes Accumulation in the Trans-Golgi Network, a Site of Virus Envelopment and Sorting of Virions to Cell Junctions. *Journal of Virology* **2001**, *75*, 1928–1940, doi:10.1128/jvi.75.4.1928-1940.2001.
21. Whiteley, A.; Bruun, B.; Minson, T.; Browne, H. Effects of Targeting Herpes Simplex Virus Type 1 gD to the Endoplasmic Reticulum and Trans-Golgi Network. *J Virol* **1999**, *73*, 9515–9520, doi:10.1128/JVI.73.11.9515-9520.1999.
22. Zhu, Z.; Gershon, M.D.; Hao, Y.; Ambron, R.T.; Gabel, C.A.; Gershon, A.A. Envelopment of Varicella-Zoster Virus: Targeting of Viral Glycoproteins to the Trans-Golgi Network. *J Virol* **1995**, *69*, 7951–7959, doi:10.1128/JVI.69.12.7951-7959.1995.
23. Hollinshead, M.; Johns, H.L.; Sayers, C.L.; Gonzalez-Lopez, C.; Smith, G.L.; Elliott, G. Endocytic Tubules Regulated by Rab GTPases 5 and 11 Are Used for Envelopment of Herpes Simplex Virus. *EMBO J* **2012**, *31*, 4204–4220, doi:10.1038/emboj.2012.262.
24. Radsak, K.; Eickmann, M.; Mockenhaupt, T.; Bogner, E.; Kern, H.; Eis-Hübinger, A.; Reschke, M. Retrieval of Human Cytomegalovirus Glycoprotein B from the Infected Cell Surface for Virus Envelopment. *Archives of Virology* **1996**, *141*, 557–572, doi:10.1007/BF01718317.
25. Krzyzaniak, M.A.; Mach, M.; Britt, W.J. HCMV-Encoded Glycoprotein M (UL100) Interacts with Rab11 Effector Protein FIP4. *Traffic* **2009**, *10*, 1439–1457, doi:10.1111/j.1600-0854.2009.00967.x.
26. Dietz, A.N.; Villinger, C.; Becker, S.; Frick, M.; Von Einem, J. A Tyrosine-Based Trafficking Motif of the Tegument Protein pUL71 Is Crucial for Human Cytomegalovirus Secondary Envelopment. *J Virol* **2018**, *92*, e00907-17, doi:10.1128/JVI.00907-17.
27. Tugizov, S.; Maidji, E.; Xiao, J.; Pereira, L. An Acidic Cluster in the Cytosolic Domain of Human Cytomegalovirus Glycoprotein B Is a Signal for Endocytosis from the Plasma Membrane. *J Virol* **1999**, *73*, 8677–8688, doi:10.1128/JVI.73.10.8677-8688.1999.
28. Archer, M.A.; Brechtel, T.M.; Davis, L.E.; Parmar, R.C.; Hasan, M.H.; Tandon, R. Inhibition of Endocytic Pathways Impacts Cytomegalovirus Maturation. *Sci Rep* **2017**, *7*, 46069, doi:10.1038/srep46069.
29. Štimac, I.; Jug Vučko, N.; Blagojević Zagorac, G.; Marcelić, M.; Mahmutefendić Lučin, H.; Lučin, P. Dynamin Inhibitors Prevent the Establishment of the Cytomegalovirus Assembly Compartment in the Early Phase of Infection. *Life (Basel)* **2021**, *11*, 876, doi:10.3390/life11090876.
30. Hasan, M.H.; Davis, L.E.; Bollavarapu, R.K.; Mitra, D.; Parmar, R.; Tandon, R. Dynamin Is Required for Efficient Cytomegalovirus Maturation and Envelopment. *J Virol* **2018**, *92*, e01418-18, doi:10.1128/JVI.01418-18.
31. Pavelka, M.; Ellinger, A.; Debbage, P.; Loewe, C.; Vetterlein, M.; Roth, J. Endocytic Routes to the Golgi Apparatus. *Histochemistry* **1998**, *109*, 555–570, doi:10.1007/s004180050255.
32. Ellinger, A.; Vetterlein, M.; Weiss, C.; Meißlitzer-Ruppitsch, C.; Neumüller, J.; Pavelka, M. High-Pressure Freezing Combined with in Vivo-DAB-Cytochemistry: A Novel Approach for Studies of Endocytic Compartments. *Journal of Structural Biology* **2010**, *169*, 286–293, doi:10.1016/j.jsb.2009.10.011.
33. Sinzger, C.; Hahn, G.; Digel, M.; Katona, R.; Sampaio, K.L.; Messerle, M.; Hengel, H.; Koszinowski, U.; Brune, W.; Adler, B. Cloning and Sequencing of a Highly Productive, Endotheliotropic Virus Strain Derived from Human Cytomegalovirus TB40/E. *J Gen Virol* **2008**, *89*, 359–368, doi:10.1099/vir.0.83286-0.
34. Rosenke, K.; Fortunato, E.A. Bromodeoxyuridine-Labeled Viral Particles as a Tool for Visualization of the Immediate-Early Events of Human Cytomegalovirus Infection. *J Virol* **2004**, *78*, 7818–7822, doi:10.1128/JVI.78.14.7818-7822.2004.
35. Read, C.; Schauflinger, M.; Nikolaenko, D.; Walther, P.; von Einem, J. Regulation of Human Cytomegalovirus Secondary Envelopment by a C-Terminal Tetralysine Motif in pUL71. *J Virol* **2019**, *93*, e02244-18, doi:10.1128/JVI.02244-18.
36. Walther, P.; Ziegler, A. Freeze Substitution of High-Pressure Frozen Samples: The Visibility of Biological Membranes Is Improved When the Substitution Medium Contains Water. *J Microsc* **2002**, *208*, 3–10, doi:10.1046/j.1365-2818.2002.01064.x.
37. Schindelin, J.; Arganda-Carreras, I.; Frise, E.; Kaynig, V.; Longair, M.; Pietzsch, T.; Preibisch, S.; Rueden, C.; Saalfeld, S.; Schmid, B.; et al. Fiji: An Open-Source Platform for Biological-Image Analysis. *Nat Methods* **2012**, *9*, 676–682, doi:10.1038/nmeth.2019.
38. Read, C.; Walther, P.; von Einem, J. Quantitative Electron Microscopy to Study HCMV Morphogenesis. In *Human Cytomegaloviruses: Methods and Protocols*; Yurochko, A.D., Ed.; Springer US: New York, NY, 2021; pp. 265–289 ISBN 978-1-07-161111-1.

39. Nicolas Roduit JMicroVision: Image Analysis Toolbox for Measuring and Quantifying Components of High-Definition Images.
40. Bergner, T.; Zech, F.; Hirschenberger, M.; Stenger, S.; Sparrer, K.M.J.; Kirchhoff, F.; Read, C. Near-Native Visualization of SARS-CoV-2 Induced Membrane Remodeling and Virion Morphogenesis. *Viruses* **2022**, *14*, 2786, doi:10.3390/v14122786.
41. Kremer, J.R.; Mastronarde, D.N.; McIntosh, J.R. Computer Visualization of Three-Dimensional Image Data Using IMOD. *J Struct Biol* **1996**, *116*, 71–76, doi:10.1006/jsbi.1996.0013.
42. Wieland, J.; Frey, S.; Rupp, U.; Essbauer, S.; Groß, R.; Münch, J.; Walther, P. Zika Virus Replication in Glioblastoma Cells: Electron Microscopic Tomography Shows 3D Arrangement of Endoplasmic Reticulum, Replication Organelles, and Viral Ribonucleoproteins. *Histochem Cell Biol* **2021**, *156*, 527–538, doi:10.1007/s00418-021-02028-2.
43. Ranftler, C.; Auinger, P.; Meisslitzer-Ruppitsch, C.; Ellinger, A.; Neumüller, J.; Pavelka, M. Electron Microscopy of Endocytic Pathways. In *Cell Imaging Techniques: Methods and Protocols*; Taatjes, D.J., Roth, J., Eds.; Humana Press: Totowa, NJ, 2013; pp. 437–447 ISBN 978-1-62703-056-4.
44. Tu, Y.; Zhao, L.; Billadeau, D.D.; Jia, D. Endosome-to-TGN Trafficking: Organelle-Vesicle and Organelle-Organelle Interactions. *Front. Cell Dev. Biol.* **2020**, *8*, doi:10.3389/fcell.2020.00163.
45. Pavelka, M.; Neumüller, J.; Ellinger, A. Retrograde Traffic in the Biosynthetic-Secretory Route. *Histochem Cell Biol* **2008**, *129*, 277–288, doi:10.1007/s00418-008-0383-1.
46. Wang, X.; Cai, Y.; Wang, H.; Zeng, Y.; Zhuang, X.; Li, B.; Jiang, L. Trans-Golgi Network-Located AP1 Gamma Adaptins Mediate Dileucine Motif-Directed Vacuolar Targeting in Arabidopsis[C][W]. *Plant Cell* **2014**, *26*, 4102–4118, doi:10.1105/tpc.114.129759.
47. Lu, L.; Tai, G.; Hong, W. Autoantigen Golgin-97, an Effector of Arl1 GTPase, Participates in Traffic from the Endosome to the Trans-Golgi Network. *Mol Biol Cell* **2004**, *15*, 4426–4443, doi:10.1091/mbc.e03-12-0872.
48. Ponnambalam, S.; Girotti, M.; Yaspo, M.-L.; Owen, C.E.; Perry, A.C.F.; Suganuma, T.; Nilsson, T.; Fried, M.; Banting, G.; Warren, G. Primate Homologues of Rat TGN38: Primary Structure, Expression and Functional Implications. *Journal of Cell Science* **1996**, *109*, 675–685, doi:10.1242/jcs.109.3.675.
49. Jean Beltran, P.M.; Mathias, R.A.; Cristea, I.M. A Portrait of the Human Organelle Proteome In Space and Time during Cytomegalovirus Infection. *Cell Systems* **2016**, *3*, 361-373.e6, doi:10.1016/j.cels.2016.08.012.
50. Schauflinger, M.; Villinger, C.; Mertens, T.; Walther, P.; von Einem, J. Analysis of Human Cytomegalovirus Secondary Envelopment by Advanced Electron Microscopy. *Cellular Microbiology* **2013**, *15*, 305–314, doi:10.1111/cmi.12077.
51. Breton, S.; Brown, D. Cold-Induced Microtubule Disruption and Relocalization of Membrane Proteins in Kidney Epithelial Cells. *Journal of the American Society of Nephrology* **1998**, *9*, 155, doi:10.1681/ASN.V92155.
52. Jarvis, M.A.; Fish, K.N.; Söderberg-Naucler, C.; Streblow, D.N.; Meyers, H.L.; Thomas, G.; Nelson, J.A. Retrieval of Human Cytomegalovirus Glycoprotein B from Cell Surface Is Not Required for Virus Envelopment in Astrocytoma Cells. *Journal of Virology* **2002**, *76*, 5147–5155, doi:10.1128/jvi.76.10.5147-5155.2002.
53. Lučin, P.; Kareluša, L.; Blagojević Zagorac, G.; Mahmutefendić Lučin, H.; Pavišić, V.; Jug Vučko, N.; Lukanović Jurić, S.; Marcelić, M.; Lisnić, B.; Jonjić, S. Cytomegaloviruses Exploit Recycling Rab Proteins in the Sequential Establishment of the Assembly Compartment. *Front Cell Dev Biol* **2018**, *6*, 165, doi:10.3389/fcell.2018.00165.
54. Mayle, K.M.; Le, A.M.; Kamei, D.T. The Intracellular Trafficking Pathway of Transferrin. *Biochim Biophys Acta* **2012**, *1820*, 264–281, doi:10.1016/j.bbagen.2011.09.009.
55. Zhang, H.; Read, C.; Nguyen, C.C.; Siddiquey, M.N.A.; Shang, C.; Hall, C.M.; von Einem, J.; Kamil, J.P. The Human Cytomegalovirus Nonstructural Glycoprotein UL148 Reorganizes the Endoplasmic Reticulum. *mBio* **2019**, *10*, e02110-19, doi:10.1128/mBio.02110-19.
56. Vetterlein, M.; Ellinger, A.; Neumüller, J.; Pavelka, M. Golgi Apparatus and TGN during Endocytosis. *Histochem Cell Biol* **2002**, *117*, 143–150, doi:10.1007/s00418-001-0371-1.
57. Alwine, J.C. The Human Cytomegalovirus Assembly Compartment: A Masterpiece of Viral Manipulation of Cellular Processes That Facilitates Assembly and Egress. *PLOS Pathogens* **2012**, *8*, e1002878, doi:10.1371/journal.ppat.1002878.
58. Hook, L.M.; Grey, F.; Grabski, R.; Tirabassi, R.; Doyle, T.; Hancock, M.; Landais, I.; Jeng, S.; McWeeney, S.; Britt, W.; et al. Cytomegalovirus miRNAs Target Secretory Pathway Genes to Facilitate Formation of the Virion Assembly Compartment and Reduce Cytokine Secretion. *Cell Host Microbe* **2014**, *15*, 363–373, doi:10.1016/j.chom.2014.02.004.
59. Turner, D.L.; Mathias, R.A. The Human Cytomegalovirus Decathlon: Ten Critical Replication Events Provide Opportunities for Restriction. *Front. Cell Dev. Biol.* **2022**, *10*, doi:10.3389/fcell.2022.1053139.
60. Joesch, M.; Mankus, D.; Yamagata, M.; Shahbazi, A.; Schalek, R.; Suissa-Peleg, A.; Meister, M.; Lichtman, J.W.; Scheirer, W.J.; Sanes, J.R. Reconstruction of Genetically Identified Neurons Imaged by Serial-Section Electron Microscopy. *eLife* **2016**, *5*, e15015, doi:10.7554/eLife.15015.

 doi:10.20944/preprints202408.1752.v1

61. Sengupta, R.; Poderycki, M.J.; Mattoo, S. CryoAPEX – an Electron Tomography Tool for Subcellular Localization of Membrane Proteins. *J Cell Sci* **2019**, *132*, jcs222315, doi:10.1242/jcs.222315.
62. Tsang, T.K.; Bushong, E.A.; Boassa, D.; Hu, J.; Romoli, B.; Phan, S.; Dulcis, D.; Su, C.-Y.; Ellisman, M.H. High-Quality Ultrastructural Preservation Using Cryofixation for 3D Electron Microscopy of Genetically Labeled Tissues. *eLife* **2018**, *7*, e35524, doi:10.7554/eLife.35524.